IEEE Photonics Journal
An IEEE Photonics Society Publication

Open Access

Study of a Graphene Saturable Absorber Film Fabricated by the Optical Deposition Method

Volume 11, Number 6, December 2019

Xinyue Zhu
Shufen Chen

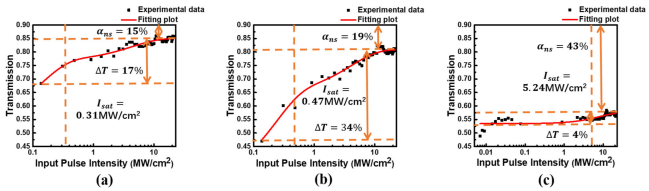

DOI: 10.1109/JPHOT.2019.2948940

IEEE photonics SOCIETY

IEEE

Study of a Graphene Saturable Absorber Film Fabricated by the Optical Deposition Method

Xinyue Zhu and Shufen Chen

School of Optics and Photonics, Beijing Institute of Technology, Beijing 100081, China

DOI:10.1109/JPHOT.2019.2948940

Manuscript received May 17, 2019; revised October 10, 2019; accepted October 18, 2019. Date of publication October 22, 2019; date of current version November 26, 2019. Corresponding author: Shufen Chen (e-mail: chensf55@sina.com).

Abstract: A film composed of graphene saturable absorber (*GSA*) prepared for a passive mode-locking (PML) fiber laser is successfully fabricated by an optical deposition method. The parameters of the process of optical deposition, including the laser intensity, deposition time and concentration of graphene solution, are investigated. Characterization of the graphene saturable absorber film, such as the modulation depth, nonsaturable loss and saturable intensity, is performed based on theoretically and experimentally optimizing the technological parameters of optical deposition. By precisely controlling the parameters of optical deposition, a *GSA* film is fabricated to satisfy the requirement of the ultra-fast pulsed fiber laser.

Index Terms: Optical deposition, graphene, saturable absorption, mode-locking fiber laser.

1. Introduction

Ultrafast pulsed lasers are essential in many application areas, such as fiber optics communication, fiber sensors and material processing. In recent research, passively mode-locked fiber lasers producing ultrashort, high power and high repetition pulses are the most suitable equipment for such commercial applications [1] due to their high beam quality, reliability, efficient heat dissipation and compact size. Furthermore, passively mode-locked fiber lasers with a saturable absorber (*SA*) are regarded to be an efficient way to generate ultrashort pulses, which are suitable for almost all applications. Traditionally, a semiconductor saturable absorber mirror (SESAM) is most commonly used as the SA [2]. However, SESAM requires a complex fabrication and packaging process and has a high cost and low damage threshold. These drawbacks of SESAM have limited the development of SAs. In recent years, the discovery of graphene with unique properties, including being wavelength-independent and having a large modulation depth, high damage threshold and ultrafast recovery time, has led to the new generation of SAs [3]–[5]. Furthermore, other SA materials, including carbon nanotubes (CNTs) [6], graphene oxide (GO) [7], reduced graphene oxide (rGO) [8], transition metal sulfides (TMSs) [9] and black phosphate [10], [11], also show similar performances as graphene. These materials have many advantages, although they also have inherent drawbacks. In general, graphene is still the most promising *SA* material. Due to the physical nature of graphene, the most common method of fabricating *GSA* in fiber system is the sandwich method [3], [4], in which the SA material is secured between two fiber ferrules connected by a fiber adaptor. To place graphene onto fiber end to fabricate *GSA*, several methods have been proposed, such as chemical vapor deposition [12], [13], polymer nanocomposite [12], [14] and optical deposition [7], [15]. Among the

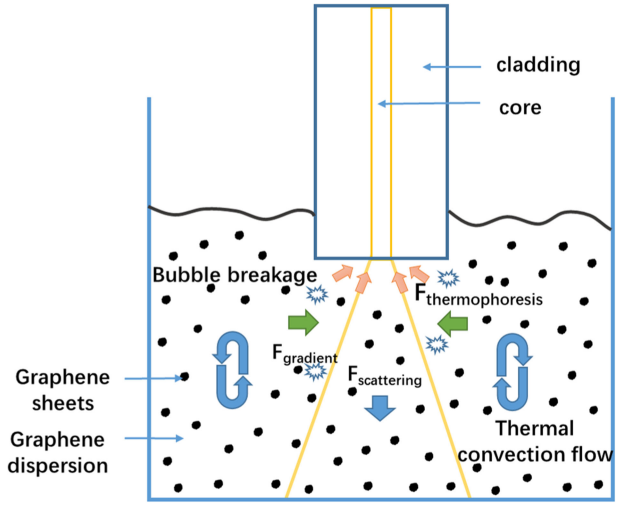

Fig. 1. Mechanism of the optical deposition of graphene.

methods mentioned above, optically driven deposition is the simplest and effective way to deposit graphene onto the fiber end. The optical deposition method was first proposed and performed to deposit carbon nanotubes in 2007 [6]. Subsequently, it was also shown that graphene could be optically deposited on the fiber end as a SA [7]. However, more detailed information about the factors that influence the process of optical deposition of graphene was not provided in early investigations.

In this paper, all the details regarding how the parameters, including the light intensity, deposition time and solution concentration, impact an optically deposited graphene film on an optical fiber end are demonstrated. The shapes of graphene films with different deposition factors were measured through a microscope. Mechanisms, including the optical trapping effect and thermal effect, are proposed to analyze the performances of different shapes of optically deposited graphene films. Furthermore, the transmission curves of the different graphene films were measured. The measured transmission curves reveal the properties of the optically deposited graphene films and indicate that different optical deposition parameters affect the optical properties of *GSA*. Finally, the variation of the optical properties of *GSA* controlled by different parameters of optical deposition are summarized. By controlling the parameters of optical deposition, *GSAs* with different properties can be produced for use in different applications.

2. Theoretical Analysis

2.1. Mechanism of the Optical Deposition of Graphene

Optical deposition is an effective way to attract graphene sheets to be deposited on a fiber end. The injected laser intensity, deposition time and solution concentration are the key parameters that influence the final result of the optical deposition. According to these parameters, there are two main mechanisms that explain the different results: the optical trapping effect (acting on the micro-particles) and the thermal effect (acting on the solution), as illustrated in Fig. 1.

Injected laser energy directly works on the graphene sheets and forces the micro graphene partials to move in a certain direction. This situation is caused by the optical trapping effect, which mainly results in two trapping forces. In the Rayleigh regime $r \ll \lambda$, according to Ref [16], the trapping forces naturally decompose into two components: The first component is the optical scattering force ($F_{scattering}$), given by

$$F_{scattering} = n_m \frac{\langle S \rangle \sigma}{c} \tag{1}$$

where σ is the scattering cross-section, $\langle S \rangle$ is the time-average Poynting vector and n_m is the index of refraction of the suspending medium. Eq. (1) shows that $F_{scattering}$ is proportional to the energy flux and points along the direction of the propagation of the incident laser beam. In fiber optically deposited systems, which are mentioned in Section 3, with an increase of the energy flux, the ($F_{gradient}$) increases and drives the micro graphene sheets away from the fiber end, which reduces the deposition of the graphene sheets on the fiber end. Therefore, at the very center of the fiber end, $F_{scattering}$ points vertically downwards, is at a very high intensity level and drives the graphene away from the fiber end, which results in thinner graphene films at the center of the fiber core. Thus, the final deposited graphene film has a ring shape when a high laser intensity is used.

The other component is the optical gradient force ($F_{gradient}$), given by

$$F_{gradient} = \frac{\alpha}{2} \nabla \langle E^2 \rangle \tag{2}$$

where α is the polarizability of the graphene particle. From Eq. (2), ($F_{gradient}$) is proportional and parallel to the gradient of the energy density. Increasing the injected laser intensity, the gradient of the energy density increases and the direction is towards the fiber core. With the increasing laser intensity, the ($F_{gradient}$) restrains the graphene sheets within the small range around the fiber core.

In the fiber optically deposited system, $F_{scattering}$ is always greater than ($F_{gradient}$). To achieve a deposited graphene film on the fiber end, there must be another influence, which is called the thermal effect, to force graphene sheets to adhere to the fiber end.

The thermal effect acts on the solution; DI water is used as the solution in the experiment, which is mentioned in Section 3. When the laser beam is injected into the graphene solution, some of the laser energy is absorbed by the DI water, resulting in different temperatures in different parts of the solution. In the laser propagation direction, the solution has a higher temperature when it is closer to the fiber end. Furthermore, the energy distribution of the laser beam is Gaussian- shaped along the radius. Therefore, the temperature gradient along the fiber radius direction points towards the fiber core. The temperature gradient results in thermal-inducing convection flow and thermophoresis force ($F_{thermophoresis}$). The direction of the thermal-inducing convection flow is not only along but also perpendicular to the propagation of the laser beam, which brings the graphene sheets into the range of the fiber core. Further, $F_{thermophoresis}$ drives the graphene sheets suspended in the solution from the hot solution to the cold fiber end core, as shown in Fig. 1.

Some of the solution is vaporized by the large amount of the energy absorbed. The vaporized liquid is confined, due to the water surface tension, and forms small bubbles in the solution. When the internal pressure of the bubble exceeds the limitation, the bubbles will explode. The force generated by this explosion will push the graphene particles to deposit on the fiber end. The higher the laser intensity, the more bubbles are in a certain range; therefore, more graphene sheets will be forced to deposit on the fiber end around the fiber core.

2.2. Properties of GSA

In mold-locking fiber laser system, SA plays a very important role to produce ultra-short pulses. According to Ref [17], the nonlinear absorption properties of SA depend on the incident laser intensity, which can be explained as follows:

$$T(I) = 1 - \Delta T \cdot \exp\left(\frac{-I}{I_{sat}}\right) - \alpha_{ns} \tag{3}$$

where $T(I)$ is the transmission, ΔT is the modulation depth, I is the input pulse energy, I_{sat} is the saturation energy (the intensity with transmission of the half the saturated value) and α_{ns} is the nonsaturable loss. As the incident laser intensity increases, the transmission of the graphene film also increases, which is shown in Fig. 2. The modulation depth, nonsaturable loss and saturation energy are the key parameters that determine the properties of SA [18]. These parameters of SA have an influence on the output performance of mode-locking lasers; many theoretical and experimental systems have been studied.

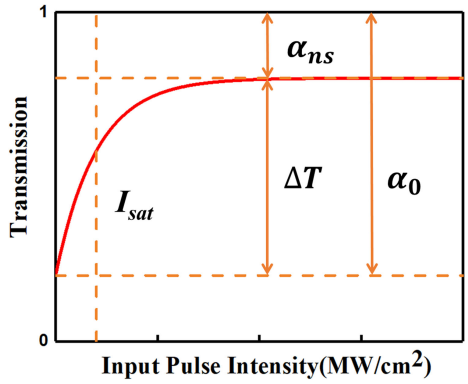

Fig. 2. Transmission curve for a saturable absorber.

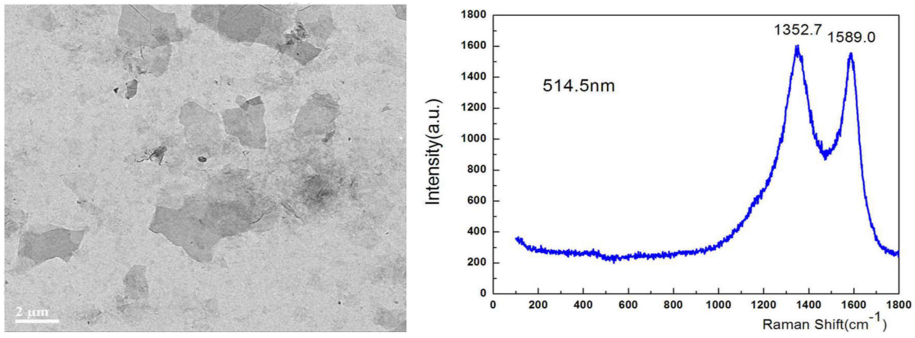

Fig. 3. (a) TEM image of dispersible graphene. (b) Raman spectrum of graphene.

3. Experimental Setup

3.1. Preparation of Graphene Solution

In the experiment, the graphene solution was prepared first. Graphene powder with a thickness from 0.8 nm to 1.2 nm (the TEM image and Raman spectrum are shown in Fig. 3; the powder was obtained from the XFNANO Company) and DI water were mixed together at a concentration of 0.5 mg/ml. Then, the mixed solution samples were subjected to long-term ultra-sonication. Under ultra-sonication for 48 hours, the aggregated graphene powder was separated into a single layer or a few layers of graphene sheets and uniformly dispersed in the *D I* water. After ultra-sonication, the pre-made solution samples were kept in an inactive state at room temperature to precipitate the remaining macroscopic flakes of graphene at the bottom of the container. Then, the supernatant of different samples was extracted to obtain the final graphene solution from different standing times. In this experiment, two different kinds of solution were obtained. The first one was obtained from a long standing time and had a low concentration, and the other one was from a short standing time and had a higher concentration than the long-standing one. In later experiments of graphene optical deposition, the solution with the higher concentration was used unless otherwise stated.

3.2. Experimental Setup for Optical Deposition

The experimental setup for optical deposition is shown in Fig. 4. A fiber laser diode (*L D*) at 980 nm generated the laser beam used for optical deposition. Then, the continuous wave traveled through the optical fiber into the 3 dB coupler (50:50) and split into two laser beams coupled into a single

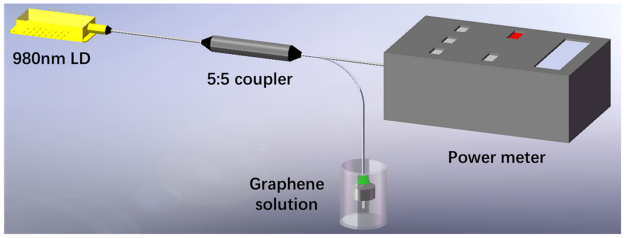

Fig. 4. Experimental setup for graphene optical deposition.

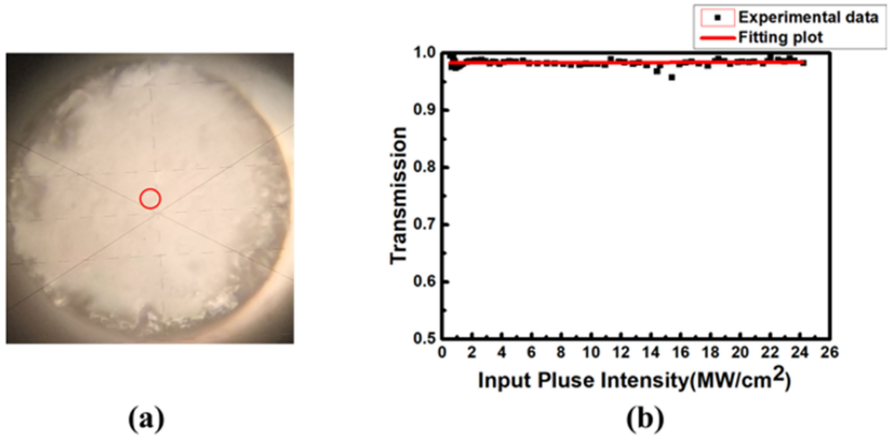

Fig. 5. (a) Image of the cleaved optical fiber end immersed in a graphene solution without injection of laser light. (b) The transmission curve of the sample shown in (a).

mode fiber (*SMF*; *CorningSMF* − 28*e* the mode field diameter 10.9 μm at 1550 nm). These two SMF are cleaved by fiber cutter to ensure the smoothness of fiber ends and then equipped with fiber ferrule. During the deposition process, one *SMF* was used to monitor the reflected power through an optical power meter. The other *SMF* was used for optical deposition, which was vertically immersed into the graphene dispersion solution. Finally, the laser beam was injected from the cleaved fiber end into the solution, driving the graphene sheets to be deposited onto the *SMF* end to fabricate *GSA* films. The shapes of the *GSA* films attached on the fiber end were measured by a microscope.The images of the fiber ends which deposited with graphene sheets and the transmission curves are presented in the next section. The images of the fiber ends are observed by microscope. The transmission curves are measured using a homemade mode-locked laser that operates at central wavelength of 1553 nm with a repetition rate of 20 MHz and a pulse duration of 500 ps.

4. Results and Discussion

Fig. 5 shows an image (a) of the fiber end and transmission curve (b) of the cleaved fiber immersed into a graphene solution for 15 min without laser injection. Fig. 5(a) shows that there is little graphene sheet aggregated on the fiber end. Meanwhile, Fig. 5(b) shows that the transmittance of the fiber is almost unchanged. Therefore, the laser is the only reason for graphene deposition in the experiment.

4.1. Influence of Light Intensity

At the same solution concentration and deposition time, different graphene films were produced by the optical deposition methods with different laser intensities. The different shapes of the graphene

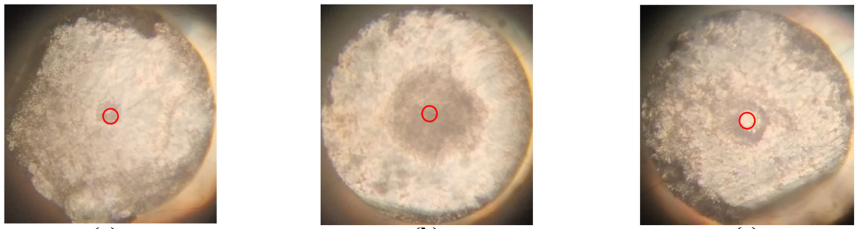

Fig. 6. Image of a graphene deposited cleaved fiber end with (a) 30 mW, (b) 50 mW, and (c) 70 mW in 5 min (the red ring is the size and position of the optical fiber core).

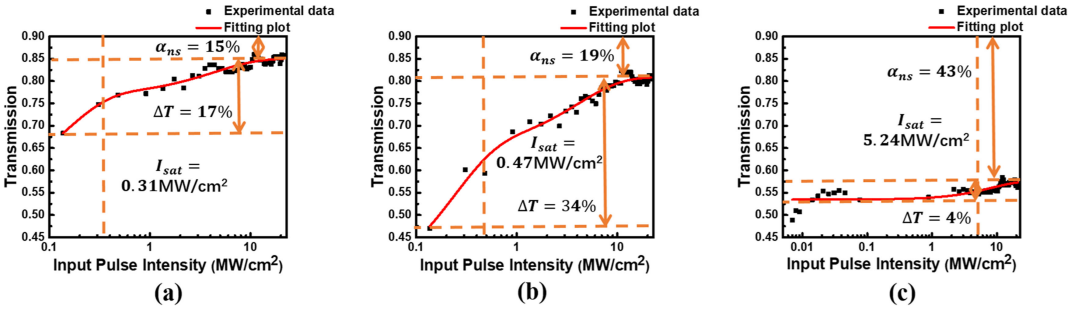

Fig. 7. Image of the transmission curve (a) 30 mW, (b) 50 mW, and (c) 70 mW in 5 min.

films are shown in Fig. 6. When the laser intensity remained at the low level, as shown in Fig. 6(a), the optically deposited graphene film was limited to the center of the fiber core. At the low-level laser intensity, the optical trapping effect and the thermal effect have little effect on the production of the graphene films; only the graphene sheets suspending near the fiber end can be deposited on the fiber core by van der Waals force. By increasing the light intensity, some of the graphene sheets are deposited on the fiber cladding, as shown in Fig. 6(b). This shape of the graphene film is caused by the thermal effect of optical deposition, including thermal flow and bubble breakage. At the very high laser intensity level, due to the Gaussian laser beam profile, $F_{scattering}$, which forces the graphene sheets away from the fiber, is much higher than that of the others, and the closer to the fiber core, the stronger $F_{scattering}$ is. Therefore, there are fewer graphene sheets deposited on the fiber core than on other parts of the fiber. Compared with the shape of the graphene film shown in Fig. 6(b), all the graphene sheets are confined in a small range around the fiber core, which is caused by the strong influence of $F_{thermophoresis}$. With the optical trapping effect and the thermal effect working together, the graphene film has a ring shape, which is shown in Fig. 6(c).

Fig. 7 shows the corresponding transmission curve of the graphene film shown in Fig. 6. From the transmission curve, the transmission rate, modulation depth and saturable intensity are discussed. Different shapes of the graphene films will have different properties. Comparing Fig. 7(a) and Fig. 7(b), with the increasingly injected laser intensity, under a certain range, the modulation depth increases and the transmission rate slightly increases, but the saturable intensity is less changed. Furthermore, the transmission curve shown in Fig. 7(c) shows a large nonsaturable loss and small modulation depth of the graphene film. Combined with Fig. 6(c), the large nonsaturable loss does not result in graphene absorption but rather in a scattering loss or damage of the graphene film from our analysis.

In general, the laser intensity has a large impact on the modulation depth; the higher the laser intensity, the larger the modulation depth. Based on Refs [19] and [20], a low modulation depth could not support the generation of pulses. Over a certain range, with the increase of the modulation depth of the SA in the fiber system, the pulse duration gradually narrows and the Time-Bandwidth

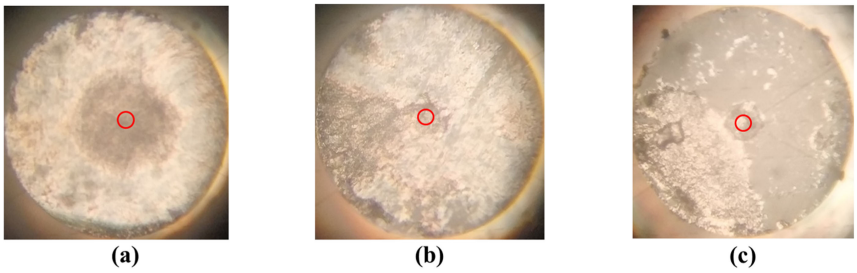

Fig. 8. Image of a graphene deposited cleaved fiber end with (a) 5 min, (b) 15 min, and (c) 30 min in 50 mW (the red ring is the size and position of the optical fiber core).

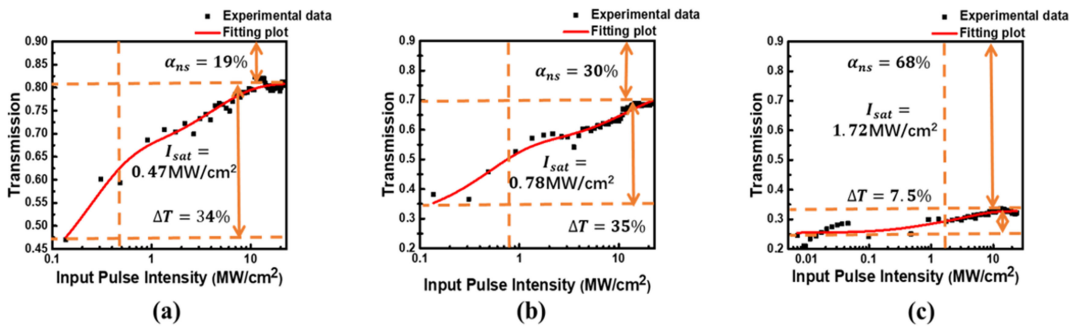

Fig. 9. Image of the transmission curve (a) 5 min, (b) 15 min, and (c) 30 min in 50 mW.

Product (*TBP*) becomes smaller (but does not reach the transform-limit), which indicates that the pulse is less chirped. However, the output peak power of the pulse decreases with the increasing modulation depth. According to this result, when the fiber system requires ultra-short pulses and there is no requirement regarding the peak power, the *GSA* produced at high intensity (under the threshold) is suitable, like a precise sensor. When there is a need for highly chirped pulses, the *GSA* produced at low intensity can be used in the fiber laser.

4.2. Influence of Deposition Time

The shapes of graphene films with different deposition times are shown in Fig. 8. Fig. 9 shows the corresponding transmission curves of the films from Fig. 8. With the increasing deposition time, an increasing amount of energy was absorbed by the solution, causing a larger temperature gradient. The high-temperature gradient increases $F_{gradient}$ and $F_{thermophoresis}$, which causes the graphene sheet to concentrate in the center of the fiber. Comparing the shape of the graphene film shown in Fig. 8(b) with that shown in Fig. 8(a), the film shown in Fig. 8(b) is more concentrated in the center. Viewing the corresponding transmission curve, which is shown in Fig. 9(b), the transmission is dramatically decreased, which indicates that the graphene film is getting thicker. The thicker graphene film is caused by a strong convection flow that drives more graphene sheets to the fiber end. As shown in Fig. 8(c) and Fig. 9(c), the graphene film in the center of the fiber end is slighting thinner, and the thicker graphene film is on the fiber cladding compared with the film shown in Fig. 8(b). This bowl shape of the graphene film is caused by the explosion force of the vaporized water bubbles around the fiber core. This force pushes the graphene sheets away from fiber core range in all directions.

According to all the analyses presented in Fig. 8 and Fig. 9, the deposition time plays an important role in the nonsaturable loss of the graphene film. The longer the deposition time, the larger the nonsaturable loss. According to the simulation results from Refs. [19] and [20], in the *PML* fiber

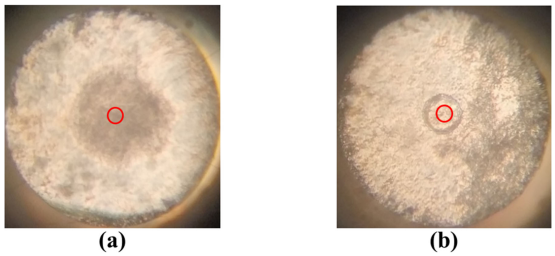

Fig. 10. Image of a graphene deposited cleaved fiber end with (a) solution with a high concentration and (b) solution with a low concentration in 50 mW, 5 min (the red ring is the size and position of the optical fiber core).

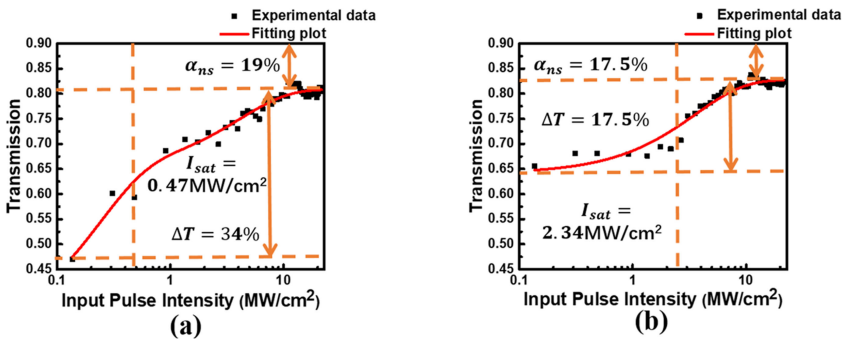

Fig. 11. Image of the transmission curve of a (a) solution with a high concentration and (b) solution with a low concentration in 50 mW, 5 min.

laser, when the nonsaturable loss increases, the peak power of the output pulse is dramatically decreased. Meanwhile, the nonsaturable loss can also slightly affect the pulse duration; the larger the nonsaturable loss, the narrower the pulse duration. Therefore, a narrow output pulse can be obtained through a long optical deposition time, but the peak power is greatly decreased. In general, the *GSA*, which is usually formed through a short deposition time, is used for the ultra-short pulse laser. However, a long-term optical deposition is sometimes used in the component of an optic limitation.

4.3. Influence of the Concentration of the Graphene Solution

The results of different solution concentrations are shown in Fig. 10. A low concentration indicates that there are fewer graphene sheets in the solution. With a low concentration solution, fewer graphene sheets are affected by the injected laser under the same laser intensity and deposition time. Therefore, under deposition with a low concentration, which is shown in Fig. 10(b), the graphene film is thinner and distributed in a small range compared with the film shown in Fig. 10(a). As shown in Fig. 11, the modulation depth and nonsaturable loss decrease and the saturable intensity increases. The effect of the decreasing solution concentration might be due to the combination of the decreasing of laser intensity and deposition time. Additionally, the graphene particles in the low concentration solution are smaller, which may be the reason for the increase in the saturable intensity.

The large saturable intensity of the *GSA* can be good for the mode-locking threshold and stability of *PML* fiber laser [21]. Therefore, a fiber laser with high stability can be achieved by the optical deposition *GSA* through a low concentration solution. Under a low concentration, the modulation depth and nonsaturable loss are also decreasing, so that the high peak power ultra-short pulse stable *PML* fiber laser would be achieved by the *GSA* with a high laser intensity, short deposition time

and low concentration. Combining different optical depositions of *GSA* parameters together, *GSAs* with different properties, which can generate different output pulses for use in different applications, can be fabricated.

5. Conclusion

In this paper, we successfully prepared a *GSA* through an optical deposition method and investigated the deposition performance and optical properties, including the modulation depth, nonsaturable loss and saturation energy. All the factors of optical deposition, including the light intensity, deposition time and solution concentration, affected the deposition performance and optical properties of the *GSA*. The laser intensity played the most important role in the modulation depth, which affected the pulse duration and chirp of the output pulses from the *PML* fiber laser. In addition, the deposition time was essential to the nonsaturable loss of the *GSA*, which contributed to the peak power of the output pulse. Meanwhile, the solution concentration had a significant impact on the saturation energy, which affected the mode-locked threshold and stability of the *PML* fiber laser. By controlling the parameters of optical deposition, the fabricated *GSA* could meet different requirements for different applications. Finally, the results of this study can be used as a guideline for researchers and technicians for the fabrication of the most suitable *GSA* through the optical deposition method.

References

[1] M. E. Fermann and I. Hartl, "Ultrafast fiber laser technology," *IEEE J. Sel. Topics Quantum Electron.*, vol. 15, no. 1, pp. 191–206, Jan. 2009.
[2] K. Ursula, "Recent developments in compact ultrafast lasers," *Nature*, vol. 424, no. 6950, pp. 831–838, 2003.
[3] T. Hasan *et al.*, "Nanotube–polymer composites for ultrafast photonics," *Adv. Mater.*, vol. 21, no. 38/39, pp. 3874–3899, 2009.
[4] Q. Bao *et al.*, "Atomic layer graphene as saturable absorber for ultrafast pulsed lasers," *Adv. Functional Mater.*, vol. 19, no. 19, pp. 3077–3083, 2010.
[5] F. Bonaccorso, "Solution processed graphene for photonics and optoelectronics," in *Proc. Nonlinear Opt.*, 2013, Paper NTh1A.1.
[6] K. Kashiwagi, S. Yamashita, and S. Y. Set, "Novel cost effective carbon nanotubes deposition technique using optical tweezer effect," *Proc. SPIE*, vol. 6478, 2007, Art. no. 64780G.
[7] M. Amos, F. Kazuyuki, X. Bo, and Y. Shinji, "Optical deposition of graphene and carbon nanotubes in a fiber ferrule for passive mode-locked lasing," *Opt. Exp.*, vol. 18, no. 22, pp. 23054–23061, 2010.
[8] S. Grzegorz *et al.*, "Graphene oxide vs. reduced graphene oxide as saturable absorbers for er-doped passively mode-locked fiber laser," *Opt. Exp.*, vol. 20, no. 17, pp. 19463–19473, 2012.
[9] W. Kangpeng *et al.*, "Ultrafast saturable absorption of two-dimensional MoS_2 nanosheets," *ACS Nano*, vol. 7, no. 10, 2013, Art. no. 9260.
[10] L. Zhi-Chao *et al.*, "Microfiber-based few-layer black phosphorus saturable absorber for ultra-fast fiber laser," *Opt. Exp.*, vol. 23, no. 15, pp. 20030–20039, 2015.
[11] F. A. A. Rashid *et al.*, "Using a black phosphorus saturable absorber to generate dual wavelengths in a q-switched ytterbium-doped fiber laser," *Laser Phys. Lett.*, vol. 13, no. 8, 2016, Art. no. 085102.
[12] H. Zhang, D. Y. Tang, L. M. Zhao, Q. L. Bao, and K. P. Loh, "Large energy mode locking of an erbium-doped fiber laser with atomic layer graphene," *Opt. Exp.*, vol. 17, no. 20, pp. 17 630–17635, 2009.
[13] L. M. Zhao, D. Y. Tang, H. Zhang, X. Wu, B. Qiaoliang, and L. Kian Ping, "Dissipative soliton operation of an ytterbium-doped fiber laser mode locked with atomic multilayer graphene," *Opt. Lett.*, vol. 35, no. 21, pp. 3622–3624, 2010.
[14] S. Zhipei *et al.*, "Graphene mode-locked ultrafast laser," *ACS Nano*, vol. 4, no. 2, pp. 803–810, 2010.
[15] H. Kim, J. Cho, S. Y. Jang, and Y. W. Song, "Deformation-immunized optical deposition of graphene for ultrafast pulsed lasers," *Appl. Phys. Lett.*, vol. 98, no. 2, 2011, Art. no. 021104.
[16] K. Svoboda and S. M. Block, "Biological applications of optical forces," *Annu. Rev. Biophys. Biomol. Struct.*, vol. 23, no. 1, pp. 247–285, 2009.
[17] F. X. Kartner, I. D. Jung, and U. Keller, "Soliton mode-locking with saturable absorbers," *IEEE J. Sel. Topics Quantum Electron.*, vol. 2, no. 3, pp. 540–556, Sep. 1996.
[18] H. A. Haus, "Mode-locking of lasers," *IEEE J. Sel. Topics Quantum Electron.*, vol. 6, no. 6, pp. 1173–1185, Nov./Dec. 2000.
[19] C. Ma, X. Tian, G. Bo, and W. Ge, "Numerical simulations on influence of the saturable absorber in er-doped fiber laser," *Opt. Commun.*, vol. 410, pp. 941–946, 2018.
[20] T. Du *et al.*, "Effects of nanomaterial saturable absorption on gain-guide soliton in a positive group-dispersion fiber laser: Simulations and experiments," *Opt. Commun.*, vol. 406, pp. 163–168, 2018.
[21] S. Yamashita, "Nonlinear optics in carbon nanotube, graphene, and related 2D materials," *APL Photon.*, vol. 4, no. 3, 2019, Art. no. 034301.